



## AMA0428, A Potent Rock Inhibitor, Attenuates Early and Late Experimental Diabetic Retinopathy

Karolien Hollanders, Inge Van Hove, Jurgen Sergeys, Tine Van Bergen, Evy Lefevere, Nele Kindt, Karolien Castermans, Evelien Vandewalle, Jos van Pelt, Lieve Moons & Ingeborg Stalmans

**To cite this article:** Karolien Hollanders, Inge Van Hove, Jurgen Sergeys, Tine Van Bergen, Evy Lefevere, Nele Kindt, Karolien Castermans, Evelien Vandewalle, Jos van Pelt, Lieve Moons & Ingeborg Stalmans (2016): AMA0428, A Potent Rock Inhibitor, Attenuates Early and Late Experimental Diabetic Retinopathy, Current Eye Research, DOI: [10.1080/02713683.2016.1183030](https://doi.org/10.1080/02713683.2016.1183030)

**To link to this article:** <http://dx.doi.org/10.1080/02713683.2016.1183030>



Published online: 11 Jul 2016.



Submit your article to this journal [↗](#)



Article views: 51



View related articles [↗](#)



View Crossmark data [↗](#)

## AMA0428, A Potent Rock Inhibitor, Attenuates Early and Late Experimental Diabetic Retinopathy

Karolien Hollanders<sup>a,b</sup>, Inge Van Hove<sup>b,a,c</sup>, Jurgen Sergeys<sup>a,c</sup>, Tine Van Bergen<sup>a</sup>, Evy Lefevere<sup>b,a,c</sup>, Nele Kindt<sup>d</sup>, Karolien Castermans<sup>d</sup>, Evelien Vandewalle<sup>a,e</sup>, Jos van Pelt<sup>f</sup>, Lieve Moons<sup>b,c</sup>, and Ingeborg Stalmans<sup>a,e</sup>

<sup>a</sup>Department of Ophthalmology, KU Leuven–University of Leuven, Leuven, Belgium; <sup>b</sup>Department of Ophthalmology, University Hospitals Ghent, Ghent, Belgium; <sup>c</sup>Department of Biology, KU Leuven–University of Leuven, Leuven, Belgium; <sup>d</sup>Amakem NV, Diepenbeek, Belgium; <sup>e</sup>Department of Ophthalmology, University Hospitals Leuven, KU Leuven–University of Leuven, Leuven, Belgium; <sup>f</sup>Department of Hepatology, University Hospitals Leuven, KU Leuven–University of Leuven, Leuven, Belgium

### ABSTRACT

**Purpose:** Diabetic retinopathy (DR) is characterized by an early stage of inflammation and vessel leakage, and an advanced vasoproliferative stage. Also, neurodegeneration might play an important role in disease pathogenesis. The aim of this study was to investigate the effect of the Rho kinase (ROCK) inhibitor, AMA0428, on these processes.

**Methods:** The response to ROCK inhibition by AMA0428 (1 µg) was studied *in vivo* using the murine model for streptozotocin (STZ)-induced diabetes, focusing on early non-proliferative DR features and the oxygen-induced retinopathy (OIR) model to investigate proliferative DR. Intravitreal (IVT) administration of AMA0428 was compared with murine anti-VEGF-R2 antibody (DC101, 6.2 µg) and placebo (H<sub>2</sub>O/PEG; 1C8). Outcome was assessed by analyzing leukostasis using fluorescein isothiocyanate coupled concanavalin A (FITC-ConA) and vessel leakage (bovine serum albumin conjugated with fluorescein isothiocyanate; FITC-BSA)/neovascularization and neurodegeneration by immunohistological approaches (hematoxylin and eosin (H&E), terminal deoxynucleotidyl transferase-mediated biotinylated UTP nick end labeling (TUNEL), Brn3a). ELISA and Western blotting were employed to unravel the consequences of ROCK inhibition (1 µM AMA0428) on myosin phosphatase target protein (MYPT)-1 phosphorylation, endothelial nitric oxide synthase (eNOS) phosphorylation, and vascular endothelial growth factor (VEGF) levels in retinas of diabetic mice, on NF-κB activity and ICAM-1 expression in endothelial cells (ECs).

**Results:** *In vivo*, AMA0428 significantly reduced vessel leakage and neovascularization, respectively, in the STZ and OIR model, comparable to DC101 therapy. Additionally, the ROCK inhibitor decreased neurodegeneration in both models and inhibited leukostasis by 30% ( $p < 0.05$ ) in the STZ model ( $p < 0.05$ ), while DC101 had no positive effect on the outcome of these latter processes. ROCK activity was upregulated in the diabetic retina and AMA0428 administration resulted in decreased phospho-MYPT-1, enhanced phospho-eNOS, and reduced VEGF levels. *In vitro*, AMA0428 interfered with NF-κB activity, thereby inhibiting ICAM-1 expression in ECs.

**Conclusions:** Targeting ROCK with AMA0428 effectively attenuated outcome in an early DR model (STZ) and a late vasoproliferative retinopathy model (OIR). These findings make AMA0428 a promising candidate with an additional anti-inflammatory and neuroprotective benefit for DR patients, as compared with anti-VEGF treatment.

### ARTICLE HISTORY

Received 13 July 2015  
Revised 7 March 2016  
Accepted 19 April 2016

### KEYWORDS



Anti-vascular endothelial growth factor; diabetic retinopathy; oxygen-induced retinopathy model; rho kinase inhibition; streptozotocin-induced retinopathy model

## Introduction

In developed countries, diabetic retinopathy (DR) is a major cause of visual impairment in the working-age population.<sup>1</sup> Due to the Western lifestyle, the number of diabetes mellitus (DM) patients expands, thereby also increasing the occurrence of DR, a frequent microvascular complication of diabetes.

Loss of vision in DR is due to changes in retinal architecture caused by abnormal angiogenesis in response to inflammation and tissue ischemia. Inflammation, a major component of diabetes, contributes to leukostasis and breakdown of the blood–retinal barrier (BRB).<sup>2,3</sup> As a result of the diabetic microvasculopathy, hypoxia increases, which itself induces neovascularization. The newly formed anomalous blood vessels cause leakage, edema, and even tractional retinal detachment, a major vision-threatening

complication in proliferative retinopathies. Besides inflammation and neovascularization, also retinal degeneration is a feature of DR.<sup>4,5</sup> Indeed, DR has several characteristics of a chronic neurodegenerative retinal disease, including changes in electrophysiological activity, neural apoptosis, and glial reactivity.<sup>4,5</sup> This disruption of neuronal output might explain why, despite effective treatment of the vascular injury, many patients still suffer from vision impairment. Moreover, findings suggest that the neurodegenerative process might start even before the development of microvasculopathy.<sup>6</sup> As such, it is obvious that the neurodegenerative process forms a critical aspect of vision loss in several retinopathies and is an important target for therapeutic intervention.

**CONTACT** Ingeborg Stalmans  [Ingeborg.Stalmans@uzleuven.be](mailto:Ingeborg.Stalmans@uzleuven.be)  Department of Ophthalmology, University Hospitals Leuven, Kapucijnenvoer 33, B-3000, Leuven, Belgium.

Karolien Hollanders and Inge Van Hove have contributed equally to this work.

Color versions of one or more of the figures in the article can be found online at [www.tandfonline.com/icey](http://www.tandfonline.com/icey).

The approved therapeutic options for proliferative retinopathies consist of destroying part of the retina by laser, in order to diminish hypoxic tissue<sup>7</sup> and/or anti-VEGF (vascular endothelial growth factor) therapy to prevent blood vessels from growing back.<sup>8</sup> Anti-VEGF injections are the first line treatment for macular edema in DR,<sup>8</sup> despite the fact that it potentially carries the risk of capillary drop-out due to pericyte regression, thereby exacerbating the ischemic process.<sup>9</sup> Furthermore, inhibition of VEGF only seems effective to a certain level, as it is mostly anti-angiogenesis driven, with only limited impact on inflammatory processes.<sup>10,11</sup> Another concern is that anti-VEGF treatment generates not only local but also systemic side effects due to regression of blood vessels and neurodegeneration.<sup>12–16</sup> Besides anti-VEGF, corticosteroids are being applied in DR, but they may cause cataract and/or glaucoma.<sup>17,18</sup> Hence, there is still a pertinent need for new treatment strategies to address the unyielding pathology of DR.

An innovative approach, targeting not only angiogenesis but also inflammation and even neurodegeneration, will be necessary for an improved outcome in visual acuity in proliferative retinopathy patients. An attractive target for candidate drugs is rho kinase (ROCK). The rho family of small GTPases controls a diverse array of cellular processes, including a number of angiogenic processes, but also inflammation.<sup>19–24</sup> Indeed, ROCK is induced by a variety of vasoactive agents, such as VEGF, resulting in endothelial hyperpermeability.<sup>25</sup> Activated RhoA/ROCK also mediates inflammation by unleashing the RelA/p65 subunit of NF- $\kappa$ B, so it can migrate to the nucleus and activate transcription of target genes including intercellular adhesion molecule-1 (ICAM-1) and several interleukins in vascular endothelial cells (ECs).<sup>26–29</sup> This increased endothelial expression of ICAM-1<sup>30,31</sup> is known to significantly increase the adherence of leukocytes to the vascular wall of retinal blood vessels in DR patients.<sup>32</sup> Notably, ROCK inhibition by fasudil was previously shown to ameliorate diabetes-induced microvascular damage by mediating an increased endothelial nitric oxide synthase (eNOS) phosphorylation, a reduced phosphorylation of myosin phosphatase target protein (MYPT)-1 and decreased ICAM-1 expression.<sup>22</sup> Furthermore, recent studies revealed that ROCK signaling is also associated with the pathogenesis of neurodegeneration<sup>33,34</sup> and suggest that ROCK inhibition could protect against neuronal damage. Indeed, ROCK inhibitors were recently reported to protect the retina against excitotoxicity,<sup>33,34</sup> as well as to augment neurite outgrowth.<sup>35–38</sup> Overall, these findings indicate the neuroprotective capacity of ROCK inhibition.

In this study, a potent and novel ROCK inhibitor, AMA0428 (Amakem Therapeutics, Diepenbeek, Belgium),<sup>39,40</sup> was investigated to gain insights into the potential therapeutic effect of ROCK inhibition on inflammatory, neoangiogenic, and neurodegenerative processes underlying DR. Overall, our data show that ROCK inhibition could be an alternative therapy for anti-VEGF in the treatment of this blinding retinopathy.

## Materials and methods

### Animals

Male C57BL/6J mice were obtained from Charles River Laboratories (L'Arbresle, Cedex, France) and Swiss foster

mothers were acquired from the KU Leuven animal facility. Housing and all experimental animal procedures were approved by the Institutional Animal Care and Research Advisory Committee of the KU Leuven, according to the 2010/63/EU Directive. All animal procedures were performed in accordance with the ARVO Statement for the Use of Animals in Ophthalmic and Vision Research, using the guidelines of our own institution.

### Compounds

In this study, the ROCK inhibitor AMA0428 (1  $\mu$ g) was tested in comparison with vehicle H<sub>2</sub>O-polyethylene glycol (PEG 400; Fagron NV, Waregem, Belgium) (both provided by Amakem Therapeutics). A positive control group was treated with the well-characterized rat anti-mouse VEGF-R2 antibody, DC101<sup>41,42</sup> (6.2  $\mu$ g), and compared with administration of an isotype-matched control antibody (1C8; 4.8  $\mu$ g; both provided by ThromboGenics NV, Heverlee, Belgium). In all experiments, the treatment groups constituted out of 10 mice and only 1 eye per mouse was used to avoid any contralateral effects.

Intravitreal (IVT) injections (1  $\mu$ l) in the different models were performed using an analytic science syringe (SGE Analytic Science, Victoria, Australia) and glass capillaries as previously described.<sup>43,44</sup>

### Streptozotocin-induced diabetic model

To investigate the *in vivo* potential of AMA0428 for the treatment of early non-proliferative DR, the streptozotocin (STZ)-induced murine model for DR was used.<sup>45</sup> C57BL/6J mice (3–5 weeks old) were rendered diabetic with five consecutive daily intraperitoneal (IP) injections of STZ (Sigma Aldrich, St. Louis, MO, USA) at 55 mg/kg, freshly dissolved in citrate buffer (pH 4.5). Development of diabetes was defined by blood glucose levels higher than 250 mg/dl and was monitored weekly after the first STZ injection (glucometer: OneTouch Vita; LifeScan, Inc., Milpitas, CA, USA). Only animals with consistently elevated glucose levels were considered diabetic. No exogenous insulin treatment was given.

Seven weeks after DM onset, mice were anesthetized with an IP injection of 60 mg/kg sodium pentobarbital (Nembutal™, CEVA, Sante Animale, Brussels, Belgium) and received an IVT injection of AMA0428 or vehicle in one eye. As a positive and negative control, another group was treated with DC101 or 1C8. Animals were sacrificed 3 days (to investigate leukostasis) or 1 week (to evaluate vessel leakage) after initiation of treatment. To check the neuroprotective properties of AMA0428, mice received an IVT injection every 2 weeks, starting from week 2 after DM onset until week 10 and were sacrificed at week 12 by cervical dislocation. Time points for treatment and sacrifice, depicted in Figure 1A, were based on the onset of DR in previously performed studies.<sup>5,45–48</sup>

### Oxygen-induced retinopathy model

The murine oxygen-induced retinopathy (OIR) model<sup>49</sup> was used to investigate the effect of ROCK inhibition on the late

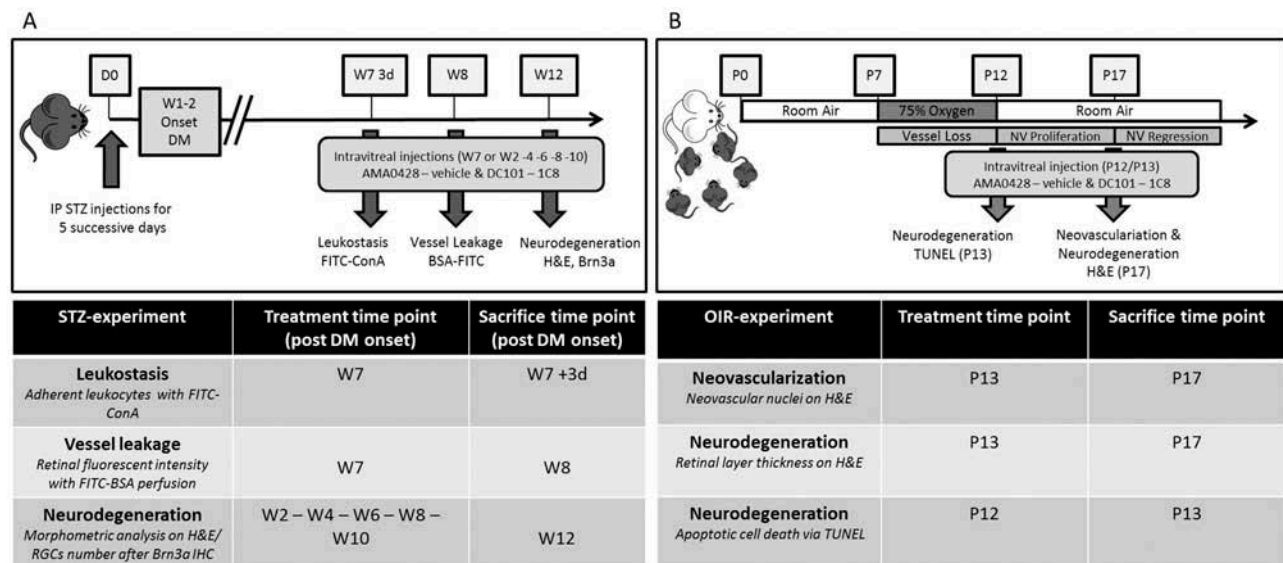


**Figure 1.** Experimental setup of the streptozotocin (STZ) and oxygen-induced retinopathy (OIR) models depicted in summarizing schemes with treatment and sacrifice time points. (A) The left panel shows a diagram of the STZ experiments in which C57BL/6J mice are rendered diabetic with five consecutive daily intraperitoneal (IP) injections. Diabetes mellitus (DM) onset was typically seen at week (W) 1 or 2 post STZ injection. (B) The right panel shows a diagram of the OIR experiments in which C57BL/6J pups with a Swiss foster mother are subjected to hyperoxia (75% oxygen) from postnatal day (P) 7 to P12, which obliterates capillaries in the retina. On P12, the animals are returned to room air, which then results in the formation of neovascular tufts, which are known to be maximal at P17, the time of sacrifice. Regression of neovascularization and normalization of the vascular pattern, which is known to occur after P17, was not studied here. FITC-ConA, fluorescein isothiocyanate coupled concanavalin A; FITC-BSA, bovine serum albumin conjugated with fluorescein isothiocyanate; H&E, hematoxylin and eosin; RGCs, retinal ganglion cells; IHC, immunohistochemical; TUNEL, terminal deoxynucleotidyl transferase-mediated biotinylated UTP nick end labeling.

stages of vasoproliferative retinopathy. Litters of 7-day-old pups (C57BL/6J) with two nursing dams (Swiss) were subjected to hyperoxia (75% oxygen) in a neonatal incubator (Inkubator-Aggregat 7011, Dräger, Wommel, Belgium) from postnatal day (P) 7 to P12. The incubator was connected to a central hospital oxygen line, allowing adjustment of oxygen concentration to  $75 \pm 2\%$ . Oxygen concentration was monitored with a MSA oxygen analyzer (MiniOX 3000, OH, USA). The cage temperature was  $28 \pm 2^\circ\text{C}$  with an air humidity of 50%. Food and water were provided *ad libitum*, but the chamber was not opened during the hyperoxia period. At P12, the animals were returned to room air (21% oxygen), which is known to cause neovascularization of the retina due to a relative hypoxia.

At P12, mice were anesthetized via an IP injection of Nembutal<sup>TM</sup> and received an IVT injection of AMA0428 or vehicle. As a positive control, another group of pups was treated with the rat anti-mouse VEGF-R2 antibody, DC101,<sup>41,42</sup> or its control antibody 1C8. Each litter was divided over the four different treatment groups, so that all treatment groups consisted of different litters, thereby circumventing a possible variable response between litters in the disease model.<sup>50</sup> Mice were sacrificed at P13 or P17 by cervical dislocation. Time points for treatment and sacrifice, all depicted in Figure 1B, were based on previously performed studies.<sup>44,49,51</sup>

### Leukostasis assay

To analyze the effect of AMA0428 on adherent retinal leukocytes in the STZ model, a perfusion labeling technique was

used, as previously reported,<sup>52</sup> with slight modifications. The retinal vasculature and adherent leukocytes were imaged with fluorescein isothiocyanate coupled concanavalin A (FITC-ConA; FL-1001, Vector Laboratories, Inc., Burlingame, CA, USA). In short, animals were deeply anesthetized with Nembutal. The chest cavity was carefully opened, and a perfusion cannula (21 gauge) was introduced into the aorta. After drainage was achieved from the right atrium, the animals were perfused for 2 min with PBS to remove erythrocytes and non-adherent leukocytes. Perfusion with FITC-ConA (40  $\mu\text{g}/\text{ml}$  in PBS; 5 mg/kg BW) was then performed to label adherent leukocytes and vascular ECs, followed by removal of residual unbound lectin with PBS perfusion for 2 min. The eyes were fixed in 1% paraformaldehyde (PFA) overnight. The next day, the retinas were carefully removed, and flat mounted on a slide containing a drop of Vectashield mounting medium (Vector Laboratories) to prevent the fluorescent dye from bleaching. The total number of adherent leukocytes in the retinal arterioles, venules, and capillaries was determined, according to Jousseaume et al.<sup>52</sup> Retinae in which the peripheral collecting vessels of the ora serrata were not visible were discarded.

### Vessel leakage assay

Vessel leakage was assessed in the STZ model at week 8 post DM onset with an approach adapted from previous studies on mice.<sup>53,54</sup> Bovine serum albumin conjugated with fluorescein isothiocyanate (FITC-BSA, 100  $\mu\text{g}/\text{g}$ , Sigma Aldrich) was injected intravenously. Thirty minutes later, the mice were sacrificed by cervical dislocation, eyes were enucleated and

placed in 4% PFA overnight followed by paraffin wax embedding. Sagittal serial sections (7  $\mu\text{m}$ ) through the central retina were collected on five microscopy slides (35  $\mu\text{m}$  between consecutive sections on one slide). Sections of one glass slide were dewaxed and vessel leakage was assessed with a fluorescence microscope on six cross-sections in total: three sections on either side of the optic nerve head (spaced 70  $\mu\text{m}$ ). So, cross-sections that included the optic nerve were excluded. Fluorescent intensities were measured on 12 nonvascular retinal images, including all retinal layers, collected in the central part of the retina (2 images of each section). The retinal fluorescent intensity per image was then normalized to the background fluorescent intensity on the slide.

### **(Immuno)histochemistry and histological analysis**

#### **Neovascularization**

To evaluate the pattern of retinal neovascularization in the OIR mouse model, mice were sacrificed at P17 and eyes were dissected and fixed overnight in 1% PFA. Before performing a hematoxylin and eosin (H&E) staining, the eyes were dehydrated (Shandon Exelsior ES; Thermo Fisher Scientific, Rochester, NY, USA), embedded in paraffin, and sagittal sections (7  $\mu\text{m}$ ) were positioned in series on five microscopy slides (35  $\mu\text{m}$  between consecutive sections on one slide). Neovascularization was investigated according to Smith et al.<sup>44,49</sup> In short, the total number of vascular nuclei, extending from the internal limiting membrane into the vitreous, was counted per retinal cross-section, on four sections on each side of the optic nerve head (eight sections per eye, spaced 35  $\mu\text{m}$ ). These vascular cell nuclei, identified under light microscopy, were considered to be associated with new vessels if they were found on the vitreal side of the internal limiting membrane. Sections that included the optic nerve head were excluded.

#### **Neurodegeneration**

The process of neurodegeneration in the STZ and the OIR model was evaluated by different (immuno)histological stainings. First, a H&E staining was performed on one series of sections to localize the optic nerve head and measure retinal layer thickness and retinal ganglion cell (RGC) density at week 12 post DM onset in the STZ model and P17 in the OIR model.

Next, within the STZ model, viable RGCs were visualized by Brn3a immunostaining at week 12 post DM onset. The serial sections were incubated overnight with goat anti-Brn3a antibody (1/750; SC31984; SantaCruz Biotechnology, Inc., Heidelberg, Germany). The next day, the slides were washed and incubated for 2 h with rabbit anti-goat (RAG)-Alexa-488 (1/200; A11078; Molecular Probes, Eugene, OR, USA). Afterward, slides were mounted with Prolong Gold with DAPI (Molecular Probes). Retinal layer thickness and RGC density were measured in the central retina at two locations, one on either side of the optic nerve. In short, digitalized images of three different serial sections (70  $\mu\text{m}$  apart) containing the optic nerve head were used (six measurements in total). To quantify RGC density, ganglion cell nuclei were counted 300  $\mu\text{m}$  from the optic nerve head on a defined length of the retina (250  $\mu\text{m}$  on either side of the optic

nerve head). These six data points were averaged for each eye and the mean values from the individual eyes were statistically analyzed. This was done both on the H&E stained and Brn3a immunostained serial sections. Alternatively, within the OIR model, terminal deoxynucleotidyl transferase-mediated biotinylated UTP nick end labeling (TUNEL) was used to detect apoptotic retinal cells at P13, a time point previously shown to be characterized by retinal cell death.<sup>51</sup> In short, serial sections were deparaffinized, rinsed, and treated with proteinase K (1/500; Qiagen, Venlo, The Netherlands) for 15 min. Next, sections were incubated with the TUNEL reaction mixture (In Situ Cell Death Detection Kit, POD; Roche, Mannheim, Germany) at 37°C for 1 h. Afterward, the slides were mounted with Prolong Gold containing DAPI (Molecular Probes). To characterize the cell loss observed in the retina of OIR mice, six sagittal sections containing the optic nerve head were scanned systematically from the temporal to the nasal ora serrata for fluorescent cells indicative of apoptosis. Positive labeled cells were counted at six serial sections/eye and averaged as number of TUNEL positive cells/section.

#### **Cells and culture conditions**

Human umbilical vein endothelial cells (HUVEC, Lonza, Walkersville, MD, USA) were cultured in 0.1% gelatin (Invitrogen, Carlsbad, CA, USA) coated T75 flasks (Sciencell Research Laboratories, Carlsbad, CA, USA). Cells were maintained in complete EGM-2 medium, supplemented with 5% fetal bovine serum (FBS, Thermo Fisher Scientific), 0.1% human recombinant epidermal growth factor, 0.4% recombinant human fibroblast growth factor, 0.1% VEGF, 0.1% recombinant lung insulin-like growth factor, 0.04% Hydrocortisone, 0.1% ascorbic acid, 0.1% heparin, and 0.1% gentamicin sulfate amphotericin-B (EBM-2 bullet kit; Lonza).

The cells were routinely maintained at 37°C in a humidified atmosphere of 5% CO<sub>2</sub> and medium was replaced every 2–3 days. Cells between third and sixth passage were used in all experiments. All *in vitro* assays were repeated at least three times in triplicate.

#### **ELISA**

##### **ROCK activity and VEGF expression levels**

To evaluate expression and activity of ROCK in the STZ model, retinas were isolated from non-diabetic control mice and from STZ-injected mice at 2, 5, 7, and 8 weeks after DM onset. To unravel the efficacy of AMA0428 for inhibiting ROCK activity and to investigate the effect of ROCK inhibition on VEGF levels, a second group of mice received an IVT injection of vehicle or AMA0428 at 7 weeks post DM onset, and retinas were dissected 3 days or 1 week later. Cell lysates from retinal samples, containing both retinas of one mouse, were obtained using the Mammalian Cell Lysis kit (Sigma-Aldrich). ROCK and VEGF levels were determined via ELISA using the ROCK Activity Assay (CSA001, Millipore, Billerica, MA, USA) and the Quantikine ELISA kit for mouse VEGF (R&D Systems, Minneapolis, MN, USA), respectively. Absorbance values were obtained with the Multiskan<sup>TM</sup> FC Microplate Photometer

(Thermo Scientific, Waltham, MA, USA) and statistically analyzed using one-way ANOVA.

### **NF- $\kappa$ B activity**

To investigate the effect of AMA0428 on the NF- $\kappa$ B pathway in HUVECs, an ELISA (Human/Mouse/Rat Phospho-RelA/NF- $\kappa$ B p65 (S536) immunoassay; R&D Systems) was used to measure phosphorylated RelA/NF- $\kappa$ B p65. In short, HUVECs were plated in a 96-well plate at a density of  $10\text{--}20 \times 10^3$  cells per well until they reached semi-confluence. Before treatment, cells were washed with PBS and incubated in serum-free medium for 0.5–1 h prior to incubation with AMA0428 (1  $\mu$ M) with or without thrombin (5 units/ml; Enzyme laboratories, South Bend, IN, USA; stimulation of HUVEC). Six hours after drug exposure, cells were fixed with 4% PFA. According to the manufacturer's instructions, primary and secondary antibody mixtures were added to each well. Finally, the fluorogenic substrates were added and fluorescence was measured (Fluorskan Ascent FL, ThermoLabsystems, Helsinki, Finland) and calculated as phosphorylated RelA/NF- $\kappa$ B p65 over total RelA/NF- $\kappa$ B p65 in the cells.

### **Western blotting**

#### **Phospho-eNOS**

The same retinal samples from STZ vehicle- and AMA0428-treated mice, used within the ROCK and VEGF ELISA, were also applied in Western blotting for detection of phospho-eNOS. Equal amounts of retinal homogenates were loaded onto 4%–12% Bis-Tris polyacrylamide gels (BioRad Laboratories, Hercules, CA, USA) and transferred to nitrocellulose membranes. Following 2 h incubation with 5% BSA and 0.1% Tween in 1 $\times$  Tris-buffered saline to avoid non-specific binding, the membrane was incubated overnight at 4°C with the rabbit polyclonal antibody anti-Phospho-eNOS (1:200, 9571, Cell Signaling, Danvers, MA, USA). After 45 min of incubation with horseradish peroxidase (HRP)-conjugated goat anti-rabbit IgG (1:20,000, DakoCytomation A/S, Copenhagen, Denmark), protein bands were visualized using the luminol-based enhanced chemiluminescent kit (SuperSignal West Dura, Thermo Scientific, Waltham, MA, USA) on the ChemiDoc MP Imaging System (BioRad Laboratories, Hercules, CA, USA). Optical density analyses were performed for the specific bands, as well as for LavaPurple (Gelcompany, San Francisco, CA, USA) total protein stain, using Image Lab 4.1 software (BioRad Laboratories, Hercules, CA, USA).

#### **ICAM-1**

Cell lysates of HUVECs at 80%–90% cell confluence were obtained. All protein concentrations were measured using the Pierce BCA Protein Assay kit (Thermo Scientific, Rochester, NY, USA). Equal amounts of protein from each sample were separated by electrophoresis using Mini-PROTEAN<sup>®</sup> TGX<sup>™</sup> Precast gels (BioRad, Temse, Belgium). Samples of non-treated and treated (1  $\mu$ M of AMA0428 with or without 5 units/ml thrombin) cell were run simultaneously on the same gel. The Trans-Blot<sup>®</sup> Turbo<sup>™</sup> Mini Nitrocellulose Transfer Packs (BioRad) were used to transfer the separated proteins by electrophoresis. Afterward, the

proteins were blocked with 5% blocking solution (milk powder) and 0.1% Tween-20 (Merck, Overijse, Belgium) in 1 $\times$  PBS for 1 h at room temperature (RT). Blots were subsequently incubated overnight at 4°C with primary rabbit polyclonal antibodies against ICAM-1 (1:200; SantaCruz Biotechnology, Inc.). The next day, the blots were rinsed and incubated for 120 min with a secondary antibody (1:5000) (HRP-conjugated pig anti-rabbit immunoglobulin, DakoCytomation A/S). Immunoreactivity was visualized using the Pierce ECL Western Blotting Substrate (Thermo Scientific). Membranes were incubated with glyceraldehyde-3-phosphate dehydrogenase (GAPDH; 1:1000; Cell Signaling) to confirm equal protein loading. Densitometric quantification of Western blot signal intensity was performed using the molecular imager ChemiDoc<sup>™</sup> XRS combined with ImageLab<sup>™</sup> Software 5.1 (BioRad) and calculated as a percentage of the mean value from non-stimulated cells.

### **Microscopy**

Vessel leakage, neovascularization, and neurodegeneration were analyzed, using a Leica microscope, equipped with a digital camera (AxioCam MrC5; Zeiss, Oberkochen, Germany), at a magnification of 20 $\times$  and a resolution of 2584  $\times$  1936 pixels. As previously described,<sup>44,55</sup> morphometric analyses were performed using commercial software (KS300; Zeiss).

The leukostasis assay was visualized using confocal imaging Laser Scanning Microscope (LSM, Olympus, Melville, NY, USA). LSM-imaging software FluoView (FV10-ASW, Olympus) was used for digital acquisition and processing of the images.

### **Statistical analysis**

All morphometric data were analyzed using the two-sided unpaired Student's *t*-test for independent samples, unless otherwise mentioned.  $p \leq 0.05$  was considered to be statistically significant. Data are represented as mean  $\pm$  SEM, unless otherwise stated. All experiments were analyzed blindly.

## **Results**

### **AMA0428 inhibited leukostasis, vessel leakage, and neurodegeneration in the STZ model**

First, we investigated the effect of AMA0428 on early non-proliferative DR features such as leukostasis and vascular permeability, within the STZ mouse model (Figure 1A). Increased leukocyte counts and ICAM-1 expression have been documented in the human retinal vasculature of eyes with DR.<sup>32</sup> Based on previous reports,<sup>46,47</sup> we checked the number of labeled-adherent leukocytes in the mouse STZ model at 7 weeks and 3 days post DM onset using FITC-ConA perfusion. STZ-induced diabetes significantly increased leukostasis in retinal vessels of diabetic, non-treated mice, as compared with non-diabetic mice. A single IVT injection with AMA0428 (1  $\mu$ g) at week 7 post DM onset decreased diabetes-enhanced leukostasis, when checked 3 days later, as shown by a significant reduction in the number of adherent leukocytes/retina by  $30.4 \pm 6.1\%$ , in comparison with vehicle-treated animals ( $p < 0.001$ ; Figure 2A,B). A single

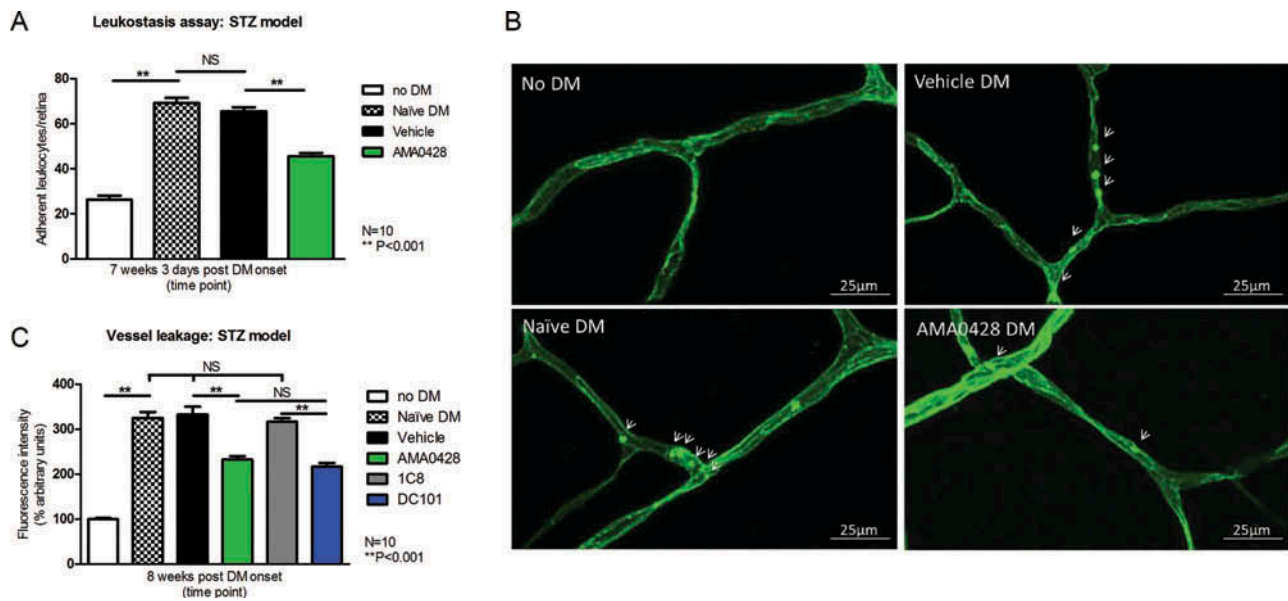


**Figure 2.** A single IVT injection of AMA0428 at 7 weeks after DM onset decreases leukocyte adhesion and retinal vessel leakage in the STZ mouse model. (A) Seven weeks and 3 days after DM onset, leukostasis was significantly increased in the STZ mouse model compared with non-diabetic mice ( $p < 0.001$ ). IVT administration of AMA0428 at 7 weeks in diabetic mice decreased leukocyte adhesion with  $30.4 \pm 6.1\%$  compared with vehicle-treated mice ( $p < 0.001$ ). (B) Representative FITC-ConA perfused flat mounts of normal/non-diabetic animals (No DM) and diabetic animals (DM) without (non-treated) or with vehicle or AMA0428 treatment. Arrowheads indicate adherent leukocytes (bar =  $25 \mu\text{m}$ ). (C) Vessel leakage, quantified at 8 weeks after DM onset, was significantly inhibited after AMA0428 administration by  $27.4 \pm 2.0\%$  compared with vehicle-treated mice ( $p < 0.05$ ); which was similar to DC101 therapy ( $32.9 \pm 2.2\%$ ). Data are represented as mean  $\pm$  SEM.

administration of DC101 ( $6.2 \mu\text{g}$ ) did not alter leukocyte adhesion in the STZ model at 3 days after single IVT injection and was found to yield similar results as the control antibody 1C8 treatment (data not shown).

Next, the effect of ROCK inhibition on blood vessel integrity, another important early process that occurs during STZ-induced experimental DR pathogenesis, was evaluated. Breakdown of the BRB characterizes early stages of vascular dysfunction in both human and experimental diabetes.<sup>56,57</sup> Within the mouse STZ model, retinal vessel leakage is known to manifest around 8 weeks after DM onset.<sup>47,53</sup> Retinal vascular permeability, measured by analyzing extravasation of FITC-BSA, showed that a single IVT injection of AMA0428 ( $1 \mu\text{g}$ ) at 7 weeks post DM onset decreased vessel leakage by  $27.4 \pm 2.0\%$ , compared with vehicle-treated mice ( $p < 0.05$ ; Figure 2C). Similarly, DC101 ( $6.2 \mu\text{g}$ ) administration inhibited vessel leakage with  $32.9 \pm 2.2\%$  as compared with its control antibody 1C8 ( $n = 10$ ,  $p < 0.05$ ).

As it has also been reported that STZ-induced diabetes results in RGC degeneration,<sup>5,48</sup> and combined with the knowledge that the neurodegenerative process might take place early in disease progress,<sup>6</sup> we additionally investigated the effect of ROCK inhibition on RGC density using H&E stained retinal sections of mice at 12 weeks after DM onset. As previously reported,<sup>5,48</sup> we also observed that the number of cells in the RGC layer of vehicle-treated eyes and naive/non-treated diabetic eyes was similarly reduced by, respectively,  $23.3 \pm 2.3\%$  and  $24.9 \pm 2.4\%$ , as compared with non-diabetic mice. Notably, morphometric analysis revealed a reduced RGC loss ( $15.3 \pm 1.8\%$ ) in mice treated every 2 weeks (week 2–4–6–8–10 after DM onset) with injections of AMA0428 ( $1 \mu\text{g}$ ), as compared with vehicle ( $p < 0.05$ , data not shown), at 12 weeks after DM onset. These results were

confirmed by Brn3a immunostaining, which showed significantly more viable RGCs when animals were treated with AMA0428 in comparison with vehicle injected diabetic eyes ( $10.5 \pm 2.0\%$ ;  $p < 0.05$ , Figure 3). Of note, DC101 and 1C8 treatment had no effect on RGC density in the STZ model (data not shown).

Overall, AMA0428 treatment attenuated leukostasis and vessel leakage, processes characterizing early non-proliferative DR. Moreover, prolonged administration of the ROCK inhibitor also improved RGC survival in the STZ model.

### AMA0428 decreased neovascularization and neurodegeneration in the OIR model

Within the STZ model, it takes months before actual neovascularization occurs.<sup>58,59</sup> Therefore, the therapeutic potential of the ROCK inhibitor AMA0428 on neo-angiogenic processes was investigated using the OIR model (Figure 1B), a well-characterized experimental model for vasoproliferative DR.<sup>49,60</sup>

Morphometric analysis on H&E serial sections disclosed that a single IVT injection of AMA0428 ( $1 \mu\text{g}$ ) at P13, 1 day upon return of the pups into normoxic conditions, significantly reduced the number of neovascular nuclei at P17, that is, by  $24.2 \pm 4.5\%$ , as compared with vehicle-treated eyes ( $p < 0.001$ ; Figure 4). This inhibitory effect of AMA0428 on angiogenesis was similar to the reduction in neoangiogenic response induced by DC101 ( $6.2 \mu\text{g}$ ) administration, that is,  $17 \pm 4.4\%$  in comparison with its control antibody 1C8.

Besides neoangiogenesis, also neurodegeneration has been described as an important feature in the OIR model.<sup>51,61</sup> Indeed, also in our experiments the retinal thickness of the central inner nuclear layer (INL) and inner plexiform layer (IPL) was found to be severely reduced in OIR mice

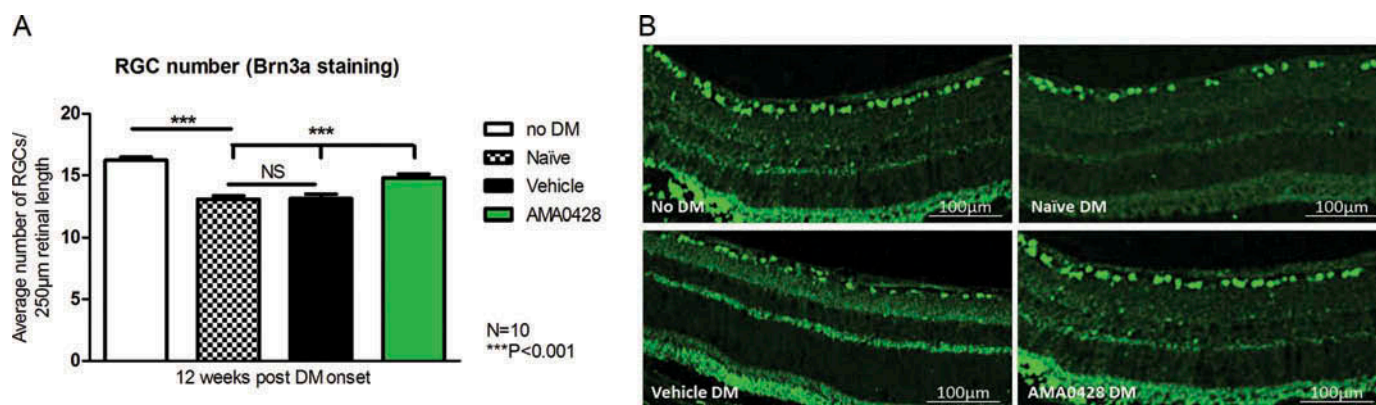


**Figure 3.** Reduced RGC loss after administration of AMA0428 in the STZ model. (A) Brn3a immunostaining showed a reduction of  $19.3 \pm 1.7\%$  of viable RGCs 12 weeks after DM onset in non-treated mice as compared with non-diabetic mice. Treatment with AMA0428 reduced RGC loss, thereby improving RGC density by  $10.5 \pm 2.0\%$  compared with vehicle-treated/non-treated diabetic mice ( $p < 0.05$ ). Data are represented as mean  $\pm$  SEM. (B) Representative pictures of the central retina (300  $\mu$ m from the optic nerve head), where viable RGCs detected by Brn3a immunostaining were counted over a distance of 250  $\mu$ m; upper left panel: no diabetes mellitus (DM); upper right panel: non-treated DM; lower left panel: DM treated with vehicle; lower right panel: DM treated with AMA0428 (bar = 100  $\mu$ m).

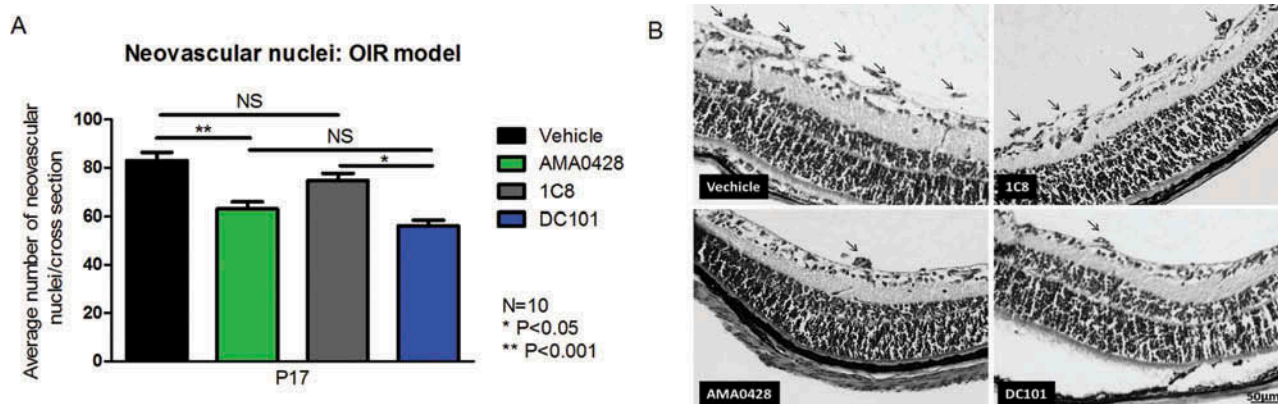


**Figure 4.** IVT administration of AMA0428 significantly reduces neovessel formation in the OIR model. (A) The number of neovascular nuclei in the OIR model is diminished by  $24.2 \pm 4.5\%$  after AMA0428 injections compared with vehicle-treated eyes ( $p < 0.001$ ), which was similar to the  $17 \pm 4.4\%$  reduction induced by DC101 in comparison with 1C8. Data are represented as mean  $\pm$  SEM. (B) Representative pictures of H&E stained serial sections at P17 of all treatment arms in the OIR experiments. Upper left panel: vehicle; lower left panel: AMA0428; upper right panel: 1C8; lower right panel: DC101. Arrows indicate neovascular tufts (bar = 50  $\mu$ m).

(respectively,  $31 \pm 3\%$  and  $32 \pm 2\%$ ; Figure 5A,B), as compared with H&E-stained retinas of room air-raised mice ( $p < 0.001$ ) at P17. Other layers (nerve fiber layer, ganglion cell layer, outer plexiform layer, outer nuclear layer, photoreceptor layer) did not significantly alter in thickness or general morphology. Importantly, single IVT administration of AMA0428 (1  $\mu$ g) at P13 resulted in a milder decrease in retinal thickness of  $10 \pm 4\%$  for the INL and  $25 \pm 4\%$  of the IPL, as compared with room air-raised mice ( $p < 0.05$ ; Figure 5A,B). Of note, DC101 (6.2  $\mu$ g) or 1C8 treatment did not affect thinning of INL and IPL (data not shown).

To further investigate whether the observed retinal thinning at P17 was caused by apoptotic cell death, a TUNEL assay was performed at P13, 24 h after return to room air and AMA0428 administration. TUNEL-positive cells were found in the central INL of untreated and vehicle-injected OIR mice. An IVT injection of pup eyes with AMA0428, however, significantly reduced the number of TUNEL-positive cells by  $33 \pm 6\%$  ( $p < 0.001$ , Figure 5C,D). Of note, the RGCs or displaced amacrine cells in the RGC layer of the ischemic retinas did not undergo cell death in our model (data not shown).

Overall, our data in the OIR model indicated that ROCK inhibition decreased neovascularization and inhibited retinal apoptotic cell death in the INL.

#### Downstream targets underlying reduced leukostasis and vessel leakage/neovascularization after inhibition of ROCK by AMA0428

##### AMA0428 inhibited NF- $\kappa$ B activity and ICAM-1 expression in ECs in vitro

In a previous report, we already showed that AMA428 administration reduced the permeability of VEGF-stimulated HUVECs,<sup>62</sup> findings that might explain the diminishing effect of this ROCK inhibitor on vessel leakage in the STZ model. Here we wished to further investigate its role in attenuating leukostasis. Diabetes is known to significantly increase the adherence of leukocytes to the vascular wall due to vascular damage and increased expression of ICAM-1 on ECs.<sup>32</sup> During vascular injury and as a result of the coagulation cascade, thrombin is formed leading to intravascular



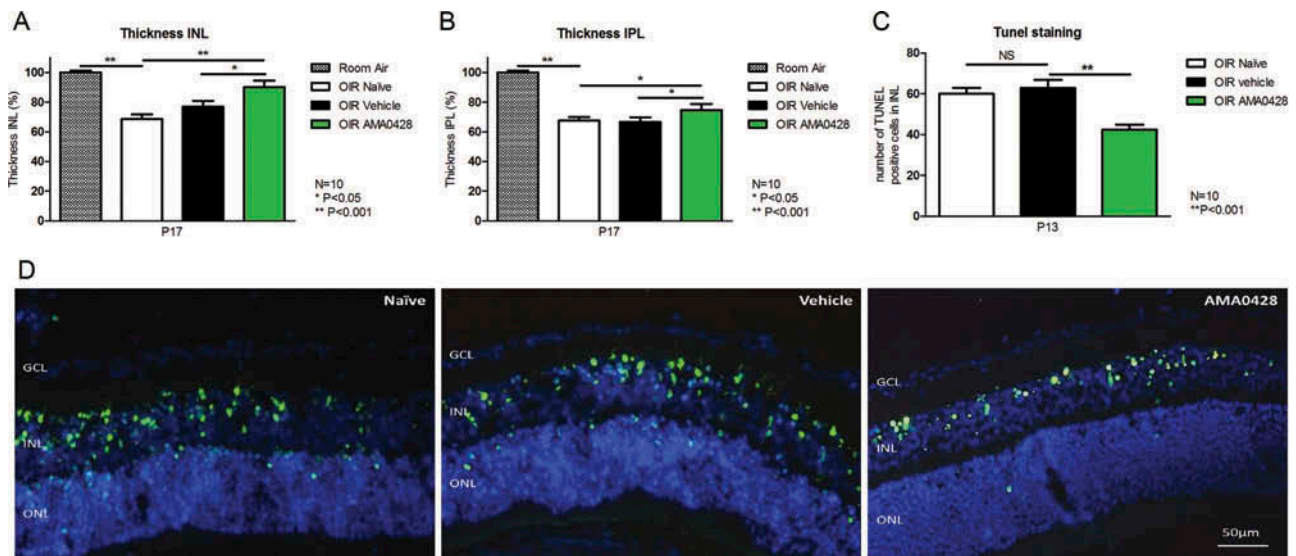


**Figure 5.** Administration of AMA0428 inhibits neuronal cell death in the OIR model. (A,B) Morphometric analysis on H&E stained sections revealed that the inner nuclear layer (INL) and inner plexiform layer (IPL) are reduced in thickness by, respectively,  $31 \pm 3\%$  (A) and  $32 \pm 2\%$  (B) in OIR mice as compared with room air-raised mice ( $p < 0.001$ ). (C) The number of TUNEL-positive cells was significantly reduced by  $33 \pm 6\%$  when AMA0428 was administered, in comparison with vehicle-/non-treated eyes ( $p < 0.001$ ). Data are represented as mean  $\pm$  SEM. (D) Representative pictures of apoptotic cells in the INL of the central P13 retina detected by TUNEL staining (green nuclei). The different retinal layers are indicated as follows: ganglion cell layer (GCL), INL, and IPL. Left panel: non-treated; middle panel: vehicle-treated; right panel: AMA0428-treated eyes (bar = 50  $\mu$ m).

coagulation,<sup>30,31</sup> but also ICAM-1 expression.<sup>27</sup> Because of the essential role of NF- $\kappa$ B in mediating thrombin-induced transcription of ICAM-1 in ECs<sup>27</sup> and the reported link between activated ROCK and the release of RelA/p65,<sup>63</sup> we investigated whether the ROCK inhibitor AMA0428 could intervene with thrombin-induced NF- $\kappa$ B activity in HUVECs. Therefore, a cell-based ELISA was performed to measure

phosphorylated RelA p65, a member of the NF- $\kappa$ B family. Indeed, thrombin challenge of HUVECs resulted in increased NF- $\kappa$ B activity, whereas exposing the cells to AMA0428 inhibited thrombin-induced NF- $\kappa$ B activity (Figure 6A). Additionally, Western blot analysis confirmed that inhibition of ROCK by AMA0428 impaired the ability of thrombin to induce ICAM-1 expression in HUVECs (Figure 6B).

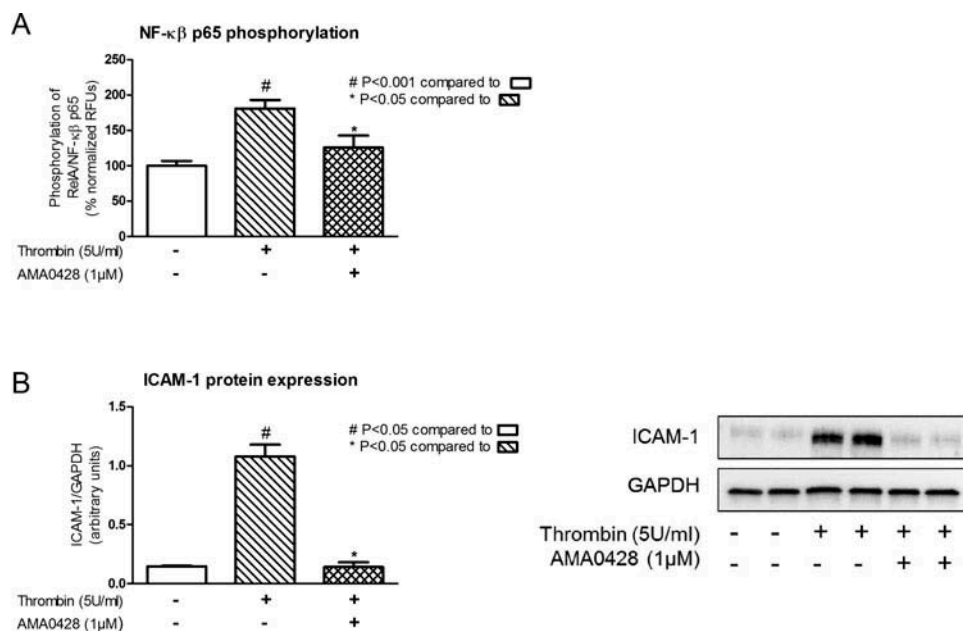


**Figure 6.** Exposure of HUVECs to AMA0428 inhibits thrombin-induced NF- $\kappa$ B activity and ICAM-1 expression. Confluent HUVEC monolayers were challenged with thrombin (5 units/ml) with/without AMA0428 (1  $\mu$ M). (A) Using a cell-based ELISA to measure phosphorylated RelA/NF- $\kappa$ B p65 an impaired ability of thrombin to induce NF- $\kappa$ B activity in HUVECs was observed after treatment with AMA0428. Bar graph represents the amount of phosphorylated over the amount of total RelA/NF- $\kappa$ B p65 and is expressed as percentage relative fluorescence units (RFUs). Data are represented as mean  $\pm$  SEM ( $n = 3$ ). (B) AMA0428 inhibits the effect of thrombin to induce ICAM-1 expression in HUVECs, as shown on the representative picture (right panel). Total cell lysates were immunoblotted with an anti-ICAM-1 antibody. The bar graph (left panel) is a representative dataset of ICAM-1 protein expression normalized to GAPDH levels (ICAM-1/GAPDH ratio in arbitrary units).

Thus, our data showed that AMA0428 intervenes with the NF- $\kappa$ B pathway, thereby inhibiting thrombin-induced ICAM-1 expression in ECs.

### AMA0428 suppressed phosphorylation of MYPT-1, increased phospho-eNOS levels, and reduced VEGF levels in the diabetic mouse retina in vivo

To confirm the contribution of the ROCK pathway in the pathology of DR previously observed in the diabetic rat retina,<sup>64</sup> an ELISA assay was used to determine ROCK activity levels in the retinas of mice subjected to the STZ model. This assay is based on phosphorylation of threonine residue 696 of MYPT-1, the major regulatory subunit of myosin phosphatase (MP) and considered a surrogate marker for ROCK activity.<sup>65</sup> ROCK levels clearly increased in the diabetic mouse retina and reached significant upregulated levels at 8 weeks post DM onset, as compared with non-diabetic animals ( $p < 0.05$ ) (Figure 7A). To investigate the efficacy of AMA0428, ROCK activity was measured in vehicle- and AMA0428-treated eyes at the time points corresponding to elevated ROCK activity in this model, more specifically, at 3 and 7 days after the IVT injection, performed at 7 weeks post DM onset. This experiment confirmed the observed increase in ROCK activity, hence MYPT-1 phosphorylation, between 7 and 8 weeks post DM onset in vehicle-treated retinas (Figure 7B) and revealed that treatment with AMA0428 significantly reduced the enhanced MYPT-1 phosphorylation in diabetic retinas (Figure 7B), thereby activating MP. As a consequence, levels of phosphorylated myosin light chain

(MLC) are supposed to diminish, which might also explain the observed reduction in leukocyte adhesion.<sup>66–69</sup>

In addition, we observed significantly increased phosphorylated, and thus activated levels of eNOS, another well-known target of ROCK, in AMA0428-treated eyes as compared with vehicle-treated or non-treated eyes at 7 weeks post DM onset (Figure 8A). These data are in line with previously published data, confirming the ability of active ROCK to (indirectly) dephosphorylate eNOS,<sup>70</sup> and thus reduce the beneficial role of eNOS in DR, which is suggested to prevent apoptosis and leukocyte adhesion.<sup>64,71–73</sup>

As VEGF is a well-known inducer of abnormal vessel growth and vessel leakage in the diabetic retina, and known to be upregulated within the STZ model,<sup>74,75</sup> VEGF levels were evaluated in vehicle- and AMA0428-treated eyes of STZ-injected mice. Figure 8B shows a clear upregulation of VEGF in the vehicle-injected diabetic retina, between 7 weeks/3 days and 8 weeks post DM onset. Moreover, application of AMA0428 at week 7 significantly reduced VEGF levels ( $p < 0.05$ ) 3 and 7 days later (Figure 8B), which can explain the diminished vessel leakage after ROCK inhibition in the STZ model.

## Discussion

The effect of a novel potent ROCK inhibitor (AMA0428) on early non-proliferative and advanced vasoproliferative DR was investigated in two different mouse models. Our results demonstrate that AMA0428 was effective in improving the

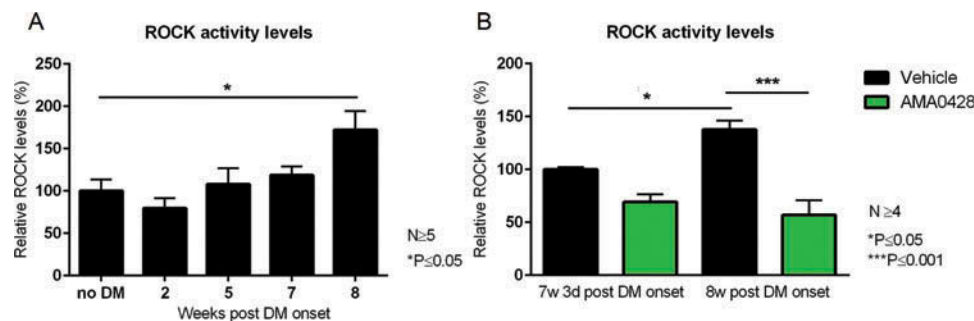


**Figure 7.** ROCK activity levels are upregulated in the retina of mice subjected to the STZ model and decreased after AMA0428 treatment. (A) ROCK activity, measured via phosphorylated MYPT-1 levels via ELISA, is clearly elevated in the retina of STZ-treated mice from 2 weeks post DM onset ( $n \geq 5$ ). (B) AMA0428 administration at 7 weeks post DM onset significantly reduced ROCK activity levels, measured 3 and 7 days later, as compared with vehicle-treated eyes ( $n \geq 4$ ). All data are represented as mean  $\pm$  SEM.

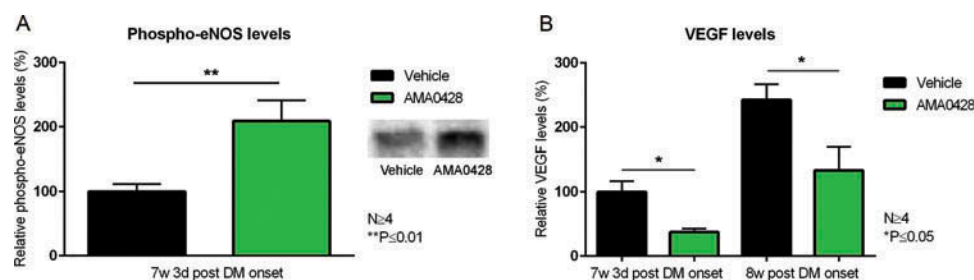


**Figure 8.** Administration of AMA0428 increases phospho-eNOS and reduces VEGF levels. (A) Western blot data on retinal samples, isolated 3 days after AMA0428 or vehicle administration at week 7 post DM onset, demonstrated clearly elevated phospho-eNOS levels in AMA0428- versus vehicle injected eyes ( $n \geq 4$ ). Representative Western blot images of both conditions are shown. Optic density values were normalized using LavaPurple total protein stain. (B) In STZ-treated mice, VEGF levels, measured via ELISA, are clearly upregulated in the vehicle-treated retina between 7 weeks/3 days and 8 weeks post DM onset. Single IVT injection of AMA0428 at weeks 2, 5, and 7 significantly lowers VEGF levels in the diabetic retina ( $n \geq 4$ ). All data are represented as mean  $\pm$  SEM and represented as a percentage relative to the vehicle-treated condition at 7 weeks/3 days post DM onset.

outcome of early DR features, like inflammation and vessel leakage, in the STZ model; as well as improving the late vasoproliferative stage as demonstrated in the OIR model. Furthermore, we directly compared the effect of AMA0428 to the well-established VEGF-R2 antibody DC101, and showed that ROCK inhibition was as effective as DC101 in reducing vessel leakage and neovascularization, with an additional inhibitory effect on inflammation and neurodegeneration.

In addition, our results showed a clear upregulation of phosphorylated MYPT-1 levels in the retina of STZ-treated mice. As MYPT-1 is an important downstream mediator of ROCK, and phosphorylation of MYPT-1 is considered a surrogate marker for ROCK activity,<sup>64,66</sup> these findings point toward enhanced levels of ROCK activity in the diabetic retina and thus, a role for the Rho/ROCK pathway in DR pathogenesis.

The present study indicated that ROCK inhibition might diminish inflammation by reducing leukostasis in the STZ-induced animal model *in vivo*, possibly due to inhibiting the expression of ICAM-1 on ECs as shown *in vitro*. Indeed, a key step for stable adhesion of leukocytes to the endothelium involves expression of ICAM-1 on the endothelial surface,<sup>76,77</sup> which is known to be significantly increased in retinal blood vessels of diabetic patients.<sup>32</sup> Activation of NF- $\kappa$ B and therefore expression of ICAM-1 is mediated by thrombin via Rho GTPase and requires alterations in actin dynamics.<sup>27</sup> In pathological conditions, such as in diabetes, thrombin is released during intravascular coagulation initiated by vascular injury.<sup>30,31</sup> Thrombin activation of RelA/p65, a subunit of NF- $\kappa$ B,<sup>78</sup> is mediated by the Rho/ROCK pathway. Indeed, phosphorylation by active ROCK is necessary in order for the RelA/p65 subunit to be released for its nuclear uptake and activate transcription of target genes including ICAM-1.<sup>27–29</sup> Inhibition of ROCK by AMA0428 impaired the ability of thrombin to induce NF- $\kappa$ B activity and ICAM-1 expression in ECs *in vitro*. These results are in line with previous reports, which employed the reference ROCK inhibitor Y-27632.<sup>27,63</sup> Indeed, the Rho/ROCK pathway, an essential mediator of NF- $\kappa$ B, is known to play a critical role in diabetic retinal microvasculopathy, since ROCK inhibition protects the vascular endothelium by blocking neutrophil adhesion.<sup>27,77</sup>

Unfortunately, Western blot data could not confirm a similar reduction in ICAM-1 levels at 3 or 7 days after AMA0428 administration at 7 weeks post DM onset, as compared with vehicle-treated retinas (data not shown). We suspect that the differences in ICAM-1 expression are too small to be detected in whole retinal tissue on Western blot, and that other leukocyte adhesion molecules, such as VCAM-1, VAP-1, or selectins, or even their binding ligands, integrins, are also involved in ROCK-mediated leukostasis.<sup>79</sup> Indeed, it has been described that phosphorylation of MLC, downstream of the Rho/ROCK pathway, is essential for assembly of integrins and controlling the high-affinity state of integrins.<sup>71,80,81</sup> Administration of AMA0428 significantly reduced phosphorylated MYPT-1 levels in the diabetic retina, thereby impeding the Rho/ROCK signaling pathway. As a consequence, levels of phosphorylated MLC are supposed to decrease, which might explain the reduction in leukocyte

adhesion.<sup>66–69,82</sup> In addition, significantly increased levels of phosphorylated and thus activated eNOS were detected in AMA0428-treated eyes as compared with vehicle-treated eyes. These data are in line with previously published data, demonstrating increased levels of phosphorylated eNOS in the retina of STZ-treated rats after administration of fasudil, another ROCK inhibitor.<sup>64,71</sup> Thus, these and previous results support the ability of active ROCK to (indirectly) dephosphorylate eNOS, and attenuate the beneficial role of eNOS in DR, for example, preventing leukocyte adhesion.<sup>64,70–73,83</sup> Overall, these data point toward the existence of multiple pathways by which the inhibition of active ROCK can result in a decreased leukocyte adhesion. The current findings also complement the previously described anti-inflammatory results of AMA0428 in the laser-induced CNV mouse model.<sup>84</sup>

In the current study, we also demonstrated that the ROCK inhibitor markedly inhibited early vessel leakage but also the later stage of neovascularization, similar to what has been observed after anti-VEGF-R2 administration in, respectively, the STZ and the OIR model. These results confirm the recently reported anti-angiogenic effect of AMA0428 in the murine laser-induced CNV model.<sup>84</sup> The Rho/ROCK signaling pathway is well-known being activated by several vasoactive agents, such as VEGF, thereby inducing endothelial hyperpermeability and angiogenesis. Notably, increasing evidence also suggests the existence of a feedback mechanism by which ROCK influences VEGF levels by interacting with VEGF-R2.<sup>85</sup> Indeed, suppression of the Rho/ROCK pathway has been demonstrated to inhibit VEGF-induced angiogenesis, by mediating EC permeability, proliferation, migration, as well as pericyte recruitment *in vitro*.<sup>25,84</sup> Moreover, we previously revealed an inhibition of VEGF upregulation by AMA0428 in mice subjected to a neovascular AMD model,<sup>84</sup> thereby inhibiting vessel leakage/neovascularization. Similarly, our current results confirm decreased VEGF levels after AMA0428 treatment in the STZ model and highlight the interplay between these two molecules in affecting blood vessel integrity and proliferation. Altogether, our and previous findings suggest that ROCK inhibition might inhibit early vessel leakage, as well as the later process of neoangiogenesis, which is important since both the breakdown of the existing BRB and the leaky nature of newly formed blood vessels are known to result in edema, a major cause of severe visual loss in DR patients.<sup>86</sup>

Importantly, it has become increasingly clear that not only the retinal vasculature but also neuronal cells are affected in DR.<sup>4,5</sup> In addition, there is some evidence that neurodegeneration might start even before the development of microangiopathy.<sup>6</sup> Therefore, we investigated this process in both experimental animal models, representing early and late changes of retinopathies and started treatment early in disease onset (week 2 after DM onset in the STZ model/immediately after return to room air in the OIR model) to have a maximal effect on the early neurodegenerative processes involved. Rodent models have been used for years to elucidate the mechanisms of retinal neuron damage in diabetes. Mohr et al.<sup>87</sup> reported increased levels of caspase activity, a marker for apoptosis, in retinas of diabetic mice, and Martin et al.<sup>48</sup> revealed that cells in

the RGC layer of the STZ-induced diabetic mouse actually undergo apoptosis. These findings were also confirmed in the present study using eyes of untreated or vehicle-treated diabetic mice. On the contrary, retinas of diabetic mice treated with AMA0428 showed significantly less apoptotic RGCs. Likewise, recent studies indicated that besides vascular pathology, neuronal injury is also a feature within the OIR model.<sup>88,89</sup> Indeed, also in our experiments, the INL and IPL were found to be reduced in thickness, without alterations in the number of RGCs. These data are in line with earlier reports,<sup>51,90</sup> and suggest that RGCs in newborn mice are better protected against ischemia compared with those in adult animals, as also described by Sennlaub et al.<sup>51</sup> Administration of AMA0428 diminished the thinning of INL and IPL in the OIR model by reducing the number of apoptotic cells in INL, pointing to a possible neuroprotective feature of ROCK inhibition. Of note, although anti-VEGF-R2 treatment did not affect retinal morphology in our study, it has been described that the currently used VEGF inhibitors might cause adverse effects linked to neuronal regression in many organs, including the eye.<sup>13,91–93</sup> Therefore, ROCK inhibition might be a safer alternative therapy for patients with proliferative retinopathies.

Overall, the present data indicate that targeting the Rho/ROCK pathway with AMA0428 efficiently reduces early DR changes, such as leukostasis and vessel leakage in the STZ model, as well as advanced DR features like neovascularization in the OIR model. Additionally, AMA0428 seems to attenuate neurodegeneration in both rodent models. These findings make AMA0428 a promising new candidate with a supplementary therapeutic benefit in the treatment of proliferative retinopathies.

## Acknowledgments

The authors thank Sofie Beckers, Ann Verbeek, Lut Noterdaeme, Lieve Geenen, and Martine Leijssen for their technical support. We thank Prof. Dr. Frederik Nevens, Prof. Dr. Schalk van der Merwe, Ingrid Vander Elst, and Petra Windmolders for their assistance in the integration of western blots. We are grateful to Prof. Dr. Jaan Toelen from the pediatric department for the use of the hyperoxygenation chamber. AMA0428 was kindly provided by Amakem Therapeutics; DC101 and IC8 were kindly provided by Thrombogenics NV.

## Declaration of interest

The authors report no conflicts of interest. The authors alone are responsible for the content and writing of the paper.

## Funding

Karolien Hollanders was financially supported by Amakem Therapeutics; Inge Van Hove was financially supported by Amakem Therapeutics via IWT Innovation fellowship; and Tine Van Bergen was financially supported by ThromboGenics NV via IWT Innovation fellowship. Nele Kindt and Karolien Castermans are employees at Amakem Therapeutics. This study was supported by a grant from the “Funds for Research in Ophthalmology” (FRO) and by the “Fund John W. Mouton Pro Retina,” which is managed by the King Baudouin Foundation for medical scientific research. Ingeborg Stalmans holds a “Chair in Ophthalmology Translational Research,” which is supported by an unrestricted grant from Amakem Therapeutics. The PhD project from Karolien Hollanders, in which this study is performed, is supported with this chair.

## ORCID

Inge Van Hove  <http://orcid.org/0000-0002-3125-0438>

Evy Lefevère  <http://orcid.org/0000-0001-8145-1070>

Lieve Moons  <http://orcid.org/0000-0003-0186-1411>

## References

1. Klein R, Klein BE, Moss SE. Epidemiology of proliferative diabetic retinopathy. *Diabetes Care* 1992;15(12):1875–1891.
2. Bresnick GH. Diabetic macular edema. A review. *Ophthalmology* 1986;93(7):989–997.
3. JM Lopes de Faria, AE Jalkh, CL Trempe, JW McMeel. Diabetic macular edema: risk factors and concomitants. *Acta Ophthalmol Scand* 1999;77(2):170–175.
4. Lieth E, Gardner TW, Barber AJ, Antonetti DA. Retinal neurodegeneration: early pathology in diabetes. *Clin Exp Ophthalmol* 2000;28(1):3–8.
5. Barber AJ. A new view of diabetic retinopathy: a neurodegenerative disease of the eye. *Prog Neuropsychopharmacol Biol Psychiatry* 2003;27(2):283–290.
6. Park SH, Park JW, Park SJ, Kim KY, Chung JW, Chun MH, et al. Apoptotic death of photoreceptors in the streptozotocin-induced diabetic rat retina. *Diabetologia* 2003;46(9):1260–1268.
7. Connolly BP, Ng EY, McNamara JA, Regillo CD, Vander JF, Tasman W. A comparison of laser photocoagulation with cryotherapy for threshold retinopathy of prematurity at 10 years: part 2. Refractive outcome. *Ophthalmology* 2002;109(5):936–941.
8. Mitchell P, Bandello F, Schmidt-Erfurth U, Lang GE, Massin P, Schlingemann RO, et al. The RESTORE study: ranibizumab monotherapy or combined with laser versus laser monotherapy for diabetic macular edema. *Ophthalmology* 2011;118(4):615–625.
9. Baffert F, Le T, Sennino B, Thurston G, Kuo CJ, Hu-Lowe D, et al. Cellular changes in normal blood capillaries undergoing regression after inhibition of VEGF signaling. *Am J Physiol. Am J Physiol Heart Circ Physiol* 2006;290(2):H547–H559.
10. Brown DM, Kaiser PK, Michels M, Soubrane G, Heier JS, Kim RY, et al. Ranibizumab versus verteporfin for neovascular age-related macular degeneration. *N Engl J Med* 2006;355(14):1432–1444.
11. Rosenfeld PJ, Brown DM, Heier JS, Boyer DS, Kaiser PK, Chung CY, et al. Ranibizumab for neovascular age-related macular degeneration. *N Engl J Med* 2006;355(14):1419–1431.
12. Tobin KA. Macugen treatment for wet age-related macular degeneration. *Insight* 2006;31(1):11–14.
13. Fraunfelder FW. Pegaptanib for wet macular degeneration. *Drugs Today (Barc)* 2005;41(11):703–709.
14. Falavarjani KG, Nguyen QD. Adverse events and complications associated with intravitreal injection of anti-VEGF agents: a review of literature. *Eye* 2013;27(7):787–794.
15. Semeraro F, Morescalchi F, Parmeggiani F, Arcidiacono B, Costagliola C. Systemic adverse drug reactions secondary to anti-VEGF intravitreal injection in patients with neovascular age-related macular degeneration. *Curr Vasc Pharmacol* 2011;9(5):629–646.
16. Iriyama A, Chen YN, Tamaki Y, Yanagi Y. Effect of anti-VEGF antibody on retinal ganglion cells in rats. *Br J Ophthalmol* 2007;91(9):1230–1233.
17. McCluskey PJ, Towler HM, Lightman S. Management of chronic uveitis. *BMJ*. 2000;320(7234):555–558.
18. Gaudio PA. A review of evidence guiding the use of corticosteroids in the treatment of intraocular inflammation. *Ocul Immunol Inflamm* 2004;12(3):169–192.
19. Danen EH, van Rheenen J, Franken W, Huveneres S, Sonneveld P, Jalink K, et al. Integrins control motile strategy through a Rho-cofilin pathway. *J Cell Biol* 2005;169(3):515–526.
20. Honjo M, Tanihara H, Kameda T, Kawaji T, Yoshimura N, Araie M. Potential role of Rho-associated protein kinase inhibitor

- Y-27632 in glaucoma filtration surgery. *Invest Ophthalmol Vis Sci* 2007;48(12):5549–5557.
21. Liu M, Gu M, Wu Y, Zhu P, Zhang W, Yin C, et al. Therapeutic effect of Y-27632 on chronic allograft nephropathy in rats. *J Surg Res* 2009;157(1):e117–e127.
  22. Arita R, Hata Y, Ishibashi T. ROCK as a therapeutic target of diabetic retinopathy. *J Ophthalmol* 2010;2010:175163.
  23. Doe C, Bentley R, Behm DJ, Lafferty R, Stavenger R, Jung D, et al. Novel Rho kinase inhibitors with anti-inflammatory and vasodilatory activities. *J Pharmacol Exp Ther* 2007;320(1):89–98.
  24. Mong PY, Wang Q. Activation of Rho kinase isoforms in lung endothelial cells during inflammation. *J Immunol* 2009;182(4):2385–2394.
  25. van Nieuw Amerongen GP, Koolwijk P, Versteilen A, van Hinsbergh VW. Involvement of RhoA/Rho kinase signaling in VEGF-induced endothelial cell migration and angiogenesis in vitro. *Arterioscler Thromb Vasc Biol* 2003;23(2):211–217.
  26. Ma Z, Zhang J, Du R, Ji E, Chu L. Rho kinase inhibition by fasudil has anti-inflammatory effects in hypercholesterolemic rats. *Biol Pharm Bull* 2011;34(11):1684–1689.
  27. Fazal F, Bijli KM, Minhajuddin M, Rein T, Finkelstein JN, Rahman A. Essential role of cofilin-1 in regulating thrombin-induced RelA/p65 nuclear translocation and intercellular adhesion molecule 1 (ICAM-1) expression in endothelial cells. *J Biol Chem* 2009;284(31):21047–21056.
  28. Rahman A, Anwar KN, Uddin S, Xu N, Ye RD, Platanius LC, et al. Protein kinase C-delta regulates thrombin-induced ICAM-1 gene expression in endothelial cells via activation of p38 mitogen-activated protein kinase. *Mol Cell Biol* 2001;21(16):5554–5565.
  29. Collins T, Read MA, Neish AS, Whitley MZ, Thanos D, Maniatis T. Transcriptional regulation of endothelial cell adhesion molecules: NF-kappa B and cytokine-inducible enhancers. *FASEB J* 1995;9(10):899–909.
  30. Aird WC. Sepsis and coagulation. *Crit Care Clin* 2005;21(3):417–431.
  31. Schouten M, Wiersinga WJ, Levi M, van der Poll T. Inflammation, endothelium, and coagulation in sepsis. *J Leukoc Biol* 2008;83(3):536–545.
  32. McLeod DS, Lefer DJ, Merges C, Lutty GA. Enhanced expression of intracellular adhesion molecule-1 and P-selectin in the diabetic human retina and choroid. *Am J Pathol* 1995;147(3):642–653.
  33. Kitaoka Y, Kumai T, Lam TT, Kuribayashi K, Isenoumi K, Munemasa Y, et al. Involvement of RhoA and possible neuroprotective effect of fasudil, a Rho kinase inhibitor, in NMDA-induced neurotoxicity in the rat retina. *Brain Res* 2004;1018(1):111–118.
  34. Jeon BT, Jeong EA, Park SY, Son H, Shin HJ, Lee DH, et al. The Rho-kinase (ROCK) inhibitor Y-27632 protects against excitotoxicity-induced neuronal death in vivo and in vitro. *Neurotox Res* 2013;23(3):238–248.
  35. Lingor P, Teusch N, Schwarz K, Mueller R, Mack H, Bahr M, et al. Inhibition of Rho kinase (ROCK) increases neurite outgrowth on chondroitin sulphate proteoglycan in vitro and axonal regeneration in the adult optic nerve in vivo. *J Neurochem* 2007;103(1):181–189.
  36. Estrach S, Schmidt S, Diriong S, Penna A, Blangy A, Fort P, et al. The Human Rho-GEF trio and its target GTPase RhoG are involved in the NGF pathway, leading to neurite outgrowth. *Curr Biol* 2002;12(4):307–312.
  37. Hove IV, Lefevre E, Moons L. ROCK inhibition as a novel potential strategy for axonal regeneration in optic neuropathies. *Neural Regen Res* 2015;10(12):1949–1950.
  38. Van de Velde S, De Groef L, Stalmans I, Moons L, Van Hove I. Towards axonal regeneration and neuroprotection in glaucoma: Rho kinase inhibitors as promising therapeutics. *Prog Neurobiol* 2015;131:105–119.
  39. Boland S, Defert O, Alen J, Bourin A, Castermans K, Kindt N, et al. 3-[2-(Aminomethyl)-5-[(pyridin-4-yl)carbomoyl]phenyl]benzoates as soft ROCK inhibitors. *Bioorg Med Chem Lett* 2013;23(23):6442–6446.
  40. Boland S, Bourin A, Alen J, Geraets J, Schroeders P, Castermans K, et al. Design, synthesis, and biological evaluation of novel, highly active soft ROCK inhibitors. *J Med Chem* 2015;58(10):4309–4324.
  41. Bocci G, Man S, Green SK, Francia G, Ebos JM, du Manoir JM, et al. Increased plasma vascular endothelial growth factor (VEGF) as a surrogate marker for optimal therapeutic dosing of VEGF receptor-2 monoclonal antibodies. *Cancer Res* 2004;64(18):6616–6625.
  42. Bocci G, Danesi R, Marangoni G, Fioravanti A, Boggi U, Esposito I, et al. Antiangiogenic versus cytotoxic therapeutic approaches to human pancreas cancer: an experimental study with a vascular endothelial growth factor receptor-2 tyrosine kinase inhibitor and gemcitabine. *Eur J Pharmacol* 2004;498(1–3):9–18.
  43. Van Bergen T, Jonckx B, Hollanders K, Sijnave D, Van de Velde S, Vandewalle E, et al. Inhibition of placental growth factor improves surgical outcome of glaucoma surgery. *J Cell Mol Med* 2013;17(12):1632–1643.
  44. Hollanders K, Van Bergen T, Van de Velde S, Sijnave D, Vandewalle E, Moons L, et al. Bevacizumab revisited: its use in different mouse models of ocular pathologies. *Curr Eye Res* 2014:1–11.
  45. Feit-Leichman RA, Kinouchi R, Takeda M, Fan Z, Mohr S, Kern TS, et al. Vascular damage in a mouse model of diabetic retinopathy: relation to neuronal and glial changes. *Invest Ophthalmol Vis Sci* 2005;46(11):4281–4287.
  46. Ishida S, Usui T, Yamashiro K, Kaji Y, Ahmed E, Carrasquillo KG, et al. VEGF164 is proinflammatory in the diabetic retina. *Invest Ophthalmol Vis Sci* 2003;44(5):2155–2162.
  47. Chen Y, Hu Y, Lin M, Jenkins AJ, Keech AC, Mott R, et al. Therapeutic effects of PPARalpha agonists on diabetic retinopathy in type 1 diabetes models. *Diabetes* 2013;62(1):261–272.
  48. Martin PM, Roon P, Van Ells TK, Ganapathy V, Smith SB. Death of retinal neurons in streptozotocin-induced diabetic mice. *Invest Ophthalmol Vis Sci* 2004;45(9):3330–3336.
  49. Smith LE, Wesolowski E, McLellan A, Kostyk SK, D'Amato R, Sullivan R, et al. Oxygen-induced retinopathy in the mouse. *Invest Ophthalmol Vis Sci* 1994;35(1):101–111.
  50. Stahl A, Connor KM, Sapieha P, Chen J, Dennison RJ, Krah NM, et al. The mouse retina as an angiogenesis model. *Invest Ophthalmol Vis Sci* 2010;51(6):2813–2826.
  51. Sennlaub F, Courtois Y, Goureau O. Inducible nitric oxide synthase mediates retinal apoptosis in ischemic proliferative retinopathy. *J Neurosci* 2002;22(10):3987–3993.
  52. Joussen AM, Murata T, Tsujikawa A, Kirchhof B, Bursell SE, Adamis AP. Leukocyte-mediated endothelial cell injury and death in the diabetic retina. *Am J Pathol* 2001;158(1):147–152.
  53. Antonetti DA, Barber AJ, Khin S, Lieth E, Tarbell JM, Gardner TW. Vascular permeability in experimental diabetes is associated with reduced endothelial occludin content: vascular endothelial growth factor decreases occludin in retinal endothelial cells. Penn State Retina Research Group. *Diabetes* 1998;47(12):1953–1959.
  54. Kim JH, Jun HO, Yu YS, Kim KW. Inhibition of protein kinase C delta attenuates blood-retinal barrier breakdown in diabetic retinopathy. *Am J Pathol* 2010;176(3):1517–1524.
  55. de Velde SV, Van Bergen T, Sijnave D, Hollanders K, Castermans K, Defert O, et al. AMA0076, a novel, locally acting rho kinase inhibitor, potentially lowers intraocular pressure in New Zealand white rabbits with minimal hyperemia. *Invest Ophthalmol Vis Sci* 2014;55(2):1006–1016.
  56. Cunha-Vaz J, Faria de Abreu JR, Campos AJ. Early breakdown of the blood-retinal barrier in diabetes. *Br J Ophthalmol* 1975;59(11):649–656.
  57. Enea NA, Hollis TM, Kern JA, Gardner TW. Histamine H1 receptors mediate increased blood-retinal barrier permeability in experimental diabetes. *Arch Ophthalmol* 1989;107(2):270–274.
  58. Kern TS, Tang J, Berkowitz BA. Validation of structural and functional lesions of diabetic retinopathy in mice. *Mol Vis* 2010;16:2121–2131.
  59. Robinson R, Barathi VA, Chaurasia SS, Wong TY, Kern TS. Update on animal models of diabetic retinopathy: from molecular

- approaches to mice and higher mammals. *Dis Model Mech* 2012;5(4):444–456.
60. Scott A, Fruttiger M. Oxygen-induced retinopathy: a model for vascular pathology in the retina. *Eye*. 2010;24(3):416–421.
  61. Narayanan SP, Suwanpradit J, Saul A, Xu Z, Still A, Caldwell RW, et al. Arginase 2 deletion reduces neuro-glial injury and improves retinal function in a model of retinopathy of prematurity. *PLoS One* 2011;6(7):e22460.
  62. Hollanders K, Van Bergen T, Kindt N, Castermans K, Leysen D, Vandewalle E, et al. The effect of AMA0428, a novel and potent ROCK inhibitor, in a model of neovascular age-related macular degeneration. *Invest Ophthalmol Vis Sci* 2015;56(2):1335–1348.
  63. Wang H, Chen X. Effects of a Rho kinase inhibitor on the sequential expression of ICAM-1, HIF-1 $\alpha$ , Bcl-2 and caspase-3 in the retina of rats with oxygen-induced retinopathy. *Int J Mol Med* 2013;32(2):457–463.
  64. Arita R, Hata Y, Nakao S, Kita T, Miura M, Kawahara S, et al. Rho kinase inhibition by fasudil ameliorates diabetes-induced microvascular damage. *Diabetes* 2009;58(1):215–226.
  65. Hartshorne DJ, Hirano K. Interactions of protein phosphatase type 1, with a focus on myosin phosphatase. *Mol Cell Biochem* 1999;190(1–2):79–84.
  66. van Nieuw Amerongen GP, Beckers CM, Achekar ID, Zeeman S, Musters RJ, van Hinsbergh VW. Involvement of Rho kinase in endothelial barrier maintenance. *Arterioscler Thromb Vasc Biol* 2007;27(11):2332–2339.
  67. Wilkinson S, Paterson HF, Marshall CJ. Cdc42-MRCK and Rho-ROCK signalling cooperate in myosin phosphorylation and cell invasion. *Nat Cell Biol* 2005;7(3):255–261.
  68. Chilcoat CD, Sharief Y, Jones SL. Tonic protein kinase A activity maintains inactive beta2 integrins in unstimulated neutrophils by reducing myosin light-chain phosphorylation: role of myosin light-chain kinase and Rho kinase. *J Leukoc Biol* 2008;83(4):964–971.
  69. Haidari M, Zhang W, Chen Z, Ganjehei L, Warier N, Vanderslice P, et al. Myosin light chain phosphorylation facilitates monocyte transendothelial migration by dissociating endothelial adherens junctions. *Cardiovasc Res* 2011;92(3):456–465.
  70. Ming XF, Viswambharan H, Barandier C, Ruffieux J, Kaibuchi K, Rusconi S, et al. Rho GTPase/Rho kinase negatively regulates endothelial nitric oxide synthase phosphorylation through the inhibition of protein kinase B/Akt in human endothelial cells. *Mol Cell Biol* 2002;22(24):8467–8477.
  71. Arita R, Nakao S, Kita T, Kawahara S, Asato R, Yoshida S, et al. A key role for ROCK in TNF- $\alpha$ -mediated diabetic microvascular damage. *Invest Ophthalmol Vis Sci* 2013;54(3):2373–2383.
  72. Prorock AJ, Hafezi-Moghadam A, Laubach VE, Liao JK, Ley K. Vascular protection by estrogen in ischemia-reperfusion injury requires endothelial nitric oxide synthase. *Am J Physiol Heart Circ Physiol* 2003;284(1):H133–H140.
  73. Srinivasan S, Hatley ME, Bolick DT, Palmer LA, Edelstein D, Brownlee M, et al. Hyperglycaemia-induced superoxide production decreases eNOS expression via AP-1 activation in aortic endothelial cells. *Diabetologia* 2004;47(10):1727–1734.
  74. Cai X, McGinnis JF. Diabetic retinopathy: animal models, therapies, and perspectives. *J Diabetes Res* 2016;2016:3789217.
  75. Garcia C, Aranda J, Arnold E, Thebault S, Macotela Y, Lopez-Casillas F, et al. Vasoinhibins prevent retinal vasopermeability associated with diabetic retinopathy in rats via protein phosphatase 2A-dependent eNOS inactivation. *J Clin Invest* 2008;118(6):2291–2300.
  76. Smith CW, Marlin SD, Rothlein R, Toman C, Anderson DC. Cooperative interactions of LFA-1 and Mac-1 with intercellular adhesion molecule-1 in facilitating adherence and transendothelial migration of human neutrophils in vitro. *J Clin Invest* 1989;83(6):2008–2017.
  77. Anwar KN, Fazal F, Malik AB, Rahman A. RhoA/Rho-associated kinase pathway selectively regulates thrombin-induced intercellular adhesion molecule-1 expression in endothelial cells via activation of I kappa B kinase beta and phosphorylation of RelA/p65. *J Immunol* 2004;173(11):6965–6972.
  78. Baldwin AS, Jr. The NF-kappa B and I kappa B proteins: new discoveries and insights. *Annu Rev Immunol* 1996;14:649–683.
  79. Noda K, Nakao S, Ishida S, Ishibashi T. Leukocyte adhesion molecules in diabetic retinopathy. *J Ophthalmol* 2012;2012:279037.
  80. Giagulli C, Scarpini E, Ottoboni L, Narumiya S, Butcher EC, Constantin G, et al. RhoA and zeta PKC control distinct modalities of LFA-1 activation by chemokines: critical role of LFA-1 affinity triggering in lymphocyte in vivo homing. *Immunity* 2004;20(1):25–35.
  81. Wolfrum S, Dendorfer A, Rikitake Y, Stalker TJ, Gong Y, Scalia R, et al. Inhibition of Rho-kinase leads to rapid activation of phosphatidylinositol 3-kinase/protein kinase Akt and cardiovascular protection. *Arterioscler Thromb Vasc Biol* 2004;24(10):1842–1847.
  82. Amano M, Ito M, Kimura K, Fukata Y, Chihara K, Nakano T, et al. Phosphorylation and activation of myosin by Rho-associated kinase (Rho-kinase). *J Biol Chem* 1996;271(34):20246–20249.
  83. Forstermann U, Munzel T. Endothelial nitric oxide synthase in vascular disease: from marvel to menace. *Circulation* 2006;113(13):1708–1714.
  84. Hollanders K, Van Bergen T, Kindt N, Castermans K, Leysen D, Vandewalle E, et al. The effect of AMA0428, a novel and potent ROCK inhibitor, in a model of neovascular age-related macular degeneration. *Invest Ophthalmol Vis Sci* 2015;56(2):1335–1348.
  85. van Nieuw Amerongen GP, van Hinsbergh VW. Role of ROCK I/II in vascular branching. *Am J Physiol Heart Circ Physiol* 2009;296(4):H903–H905.
  86. Montanez E, Wickstrom SA, Altstatter J, Chu H, Fassler R. Alpha-parvin controls vascular mural cell recruitment to vessel wall by regulating RhoA/ROCK signalling. *EMBO J* 2009;28(20):3132–3144.
  87. Mohr S, Xi X, Tang J, Kern TS. Caspase activation in retinas of diabetic and galactosemic mice and diabetic patients. *Diabetes* 2002;51(4):1172–1179.
  88. Akula JD, Mocko JA, Benador IY, Hansen RM, Favazza TL, Vyhovsky TC, et al. The neurovascular relation in oxygen-induced retinopathy. *Mol Vis* 2008;14:2499–2508.
  89. Fulton AB, Hansen RM, Moskowitz A, Akula JD. The neurovascular retina in retinopathy of prematurity. *Prog Retin Eye Res* 2009;28(6):452–482.
  90. Dorfman AL, Cuenca N, Pinilla I, Chemtob S, Lachapelle P. Immunohistochemical evidence of synaptic retraction, cytoarchitectural remodeling, and cell death in the inner retina of the rat model of oxygen-induced retinopathy (OIR). *Invest Ophthalmol Vis Sci* 2011;52(3):1693–1708.
  91. Iriyama A, Chen YN, Tamaki Y, Yanagi Y. Effect of anti-VEGF antibody on retinal ganglion cells in rats. *Br J Ophthalmol* 2007;91(9):1230–1233.
  92. Klein KS, Walsh MK, Hassan TS, Halperin LS, Castellarin AA, Roth D, et al. Endophthalmitis after anti-VEGF injections. *Ophthalmology* 2009;116(6):1225 e1.
  93. Nishijima K, Ng YS, Zhong L, Bradley J, Schubert W, Jo N, et al. Vascular endothelial growth factor-A is a survival factor for retinal neurons and a critical neuroprotectant during the adaptive response to ischemic injury. *Am J Pathol* 2007;171(1):53–67.